Additional File 1 for

Rupture processes of the 2021 and 2022 Fukushima-oki earthquakes: Adjacent events on the complex fault system in the subducting slab

Hiroaki Kobayashi[1], Tetsushi Watanabe[1], Kazuki Koketsu[2]

[1] Kobori Research Complex Inc., 6-5-30 Akasaka, Minato-ku, Tokyo, Japan.

[2] Graduate School of Media and Governance, Keio University, 5322 Endo, Fujisawa-shi, Kanagawa, Japan

Correspondence: kohiroak@kobori-takken.co.jp

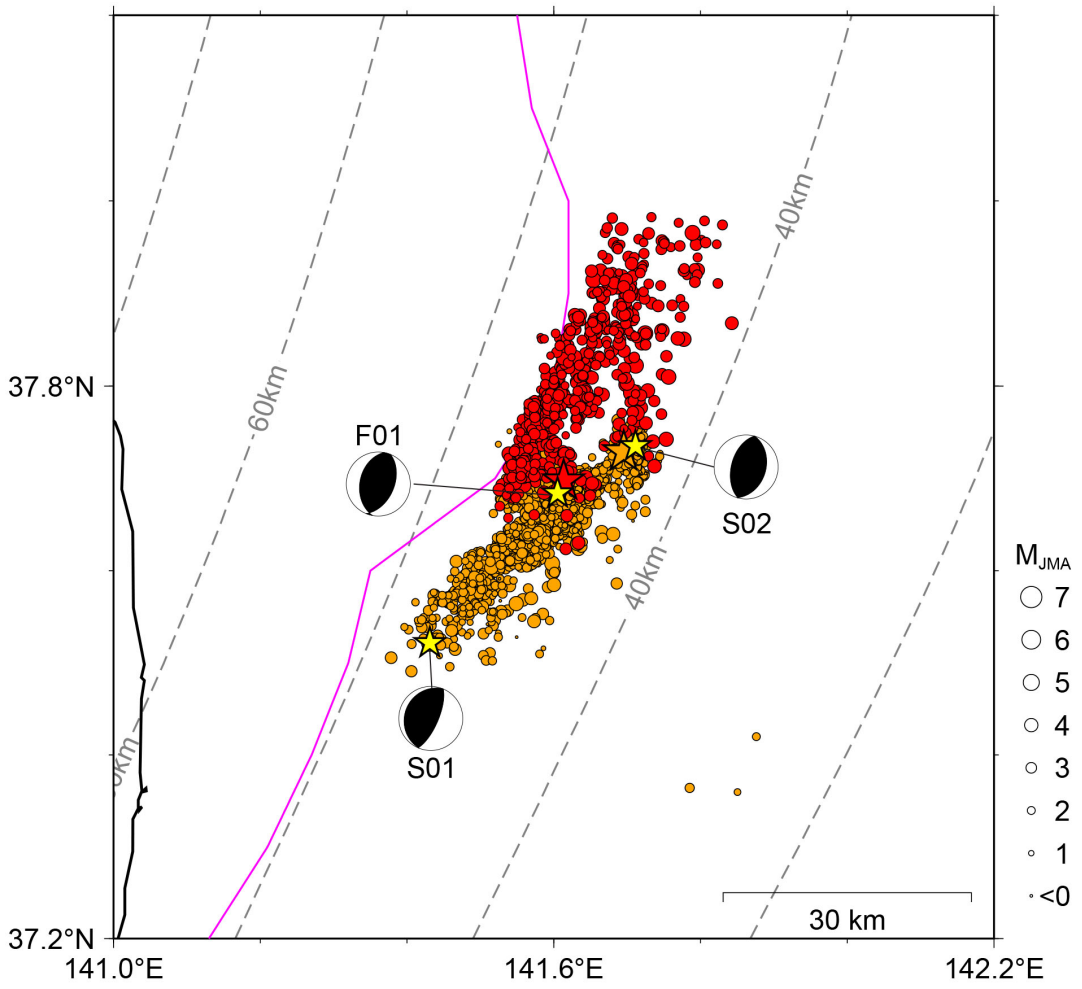

Figure S1

Distribution of events considered in this study. The yellow stars indicate the relocated epicenters of three medium-sized earthquakes (F01, S01, and S02), and their focal mechanisms are shown near the epicenters. The orange star and circles indicate the relocated epicenters of the mainshock and 24-h aftershocks, respectively, of the 2021 Fukushima-oki earthquake. The red star and circles are for the 2022 earthquake. The gray broken lines denote the plate-boundary depth at intervals of 10 km (Iwasaki et al. 2015). The pink line shows the lower depth limit of the area where interplate earthquakes occur (Igarashi et al. 2001; Uchida et al. 2009).

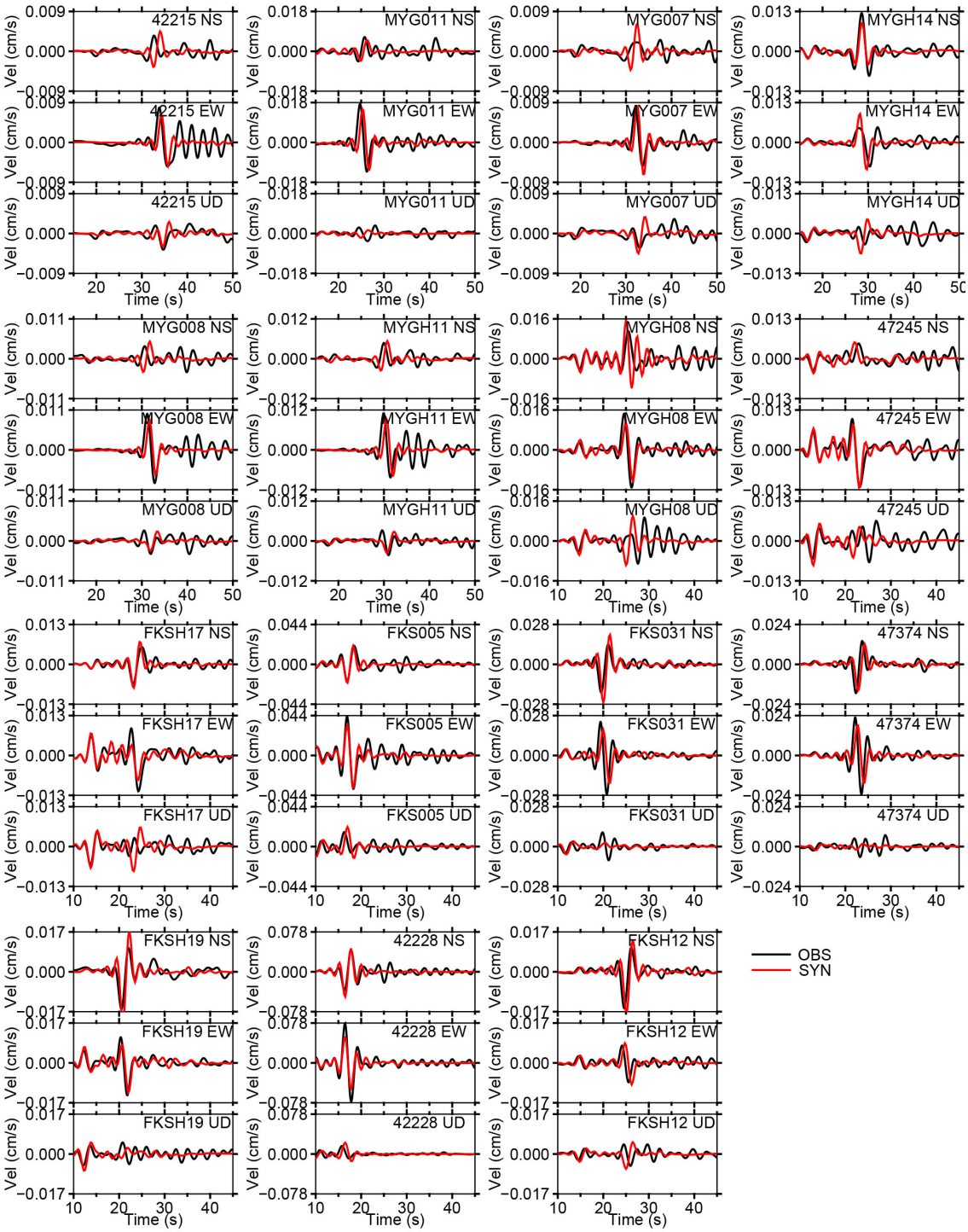

Figure S2

Observed (black) and synthetic strong motion waveforms (0.05–0.4 Hz) of event S01.

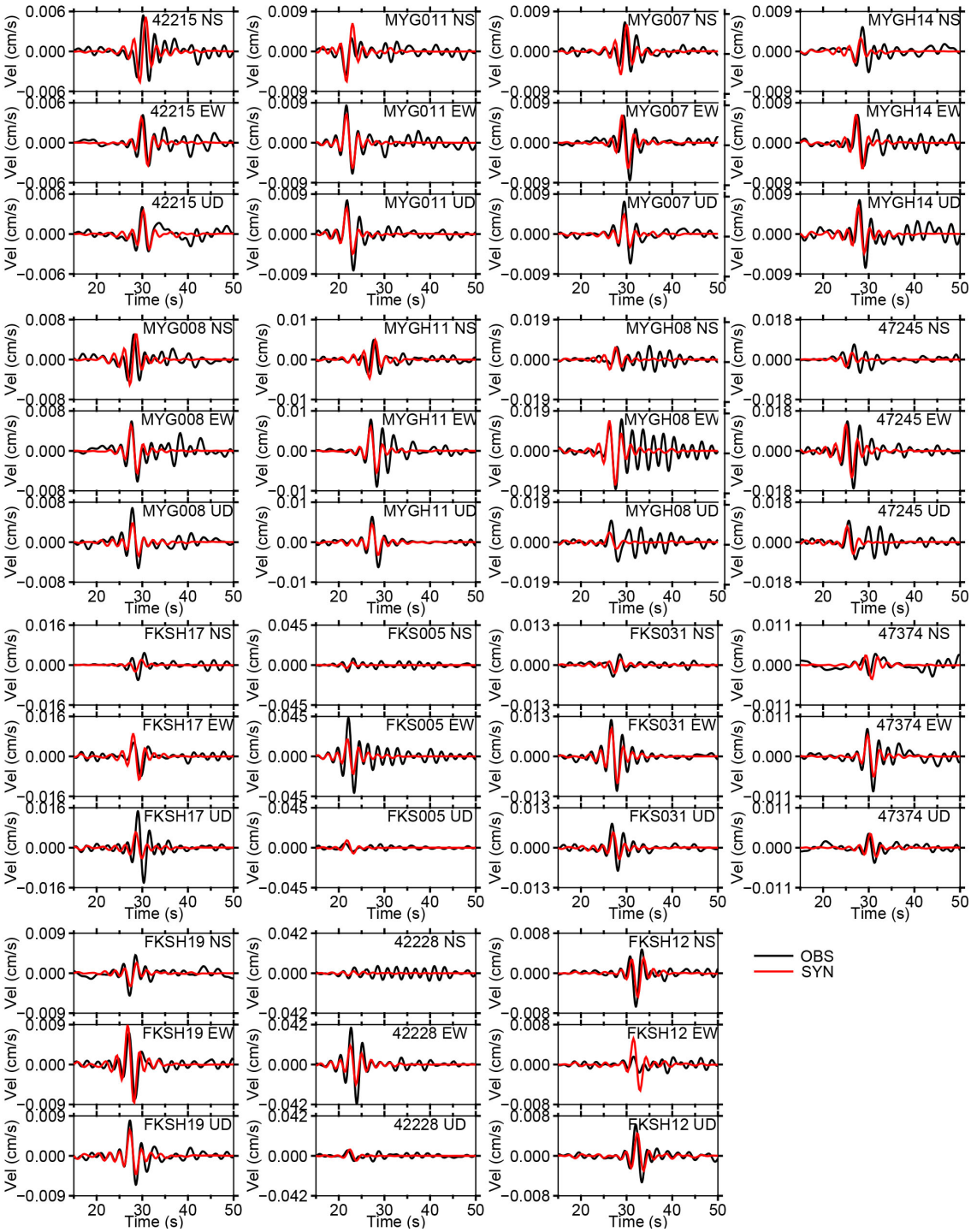

Figure S3

Observed (black) and synthetic strong motion waveforms (0.05–0.4 Hz) of event S02.

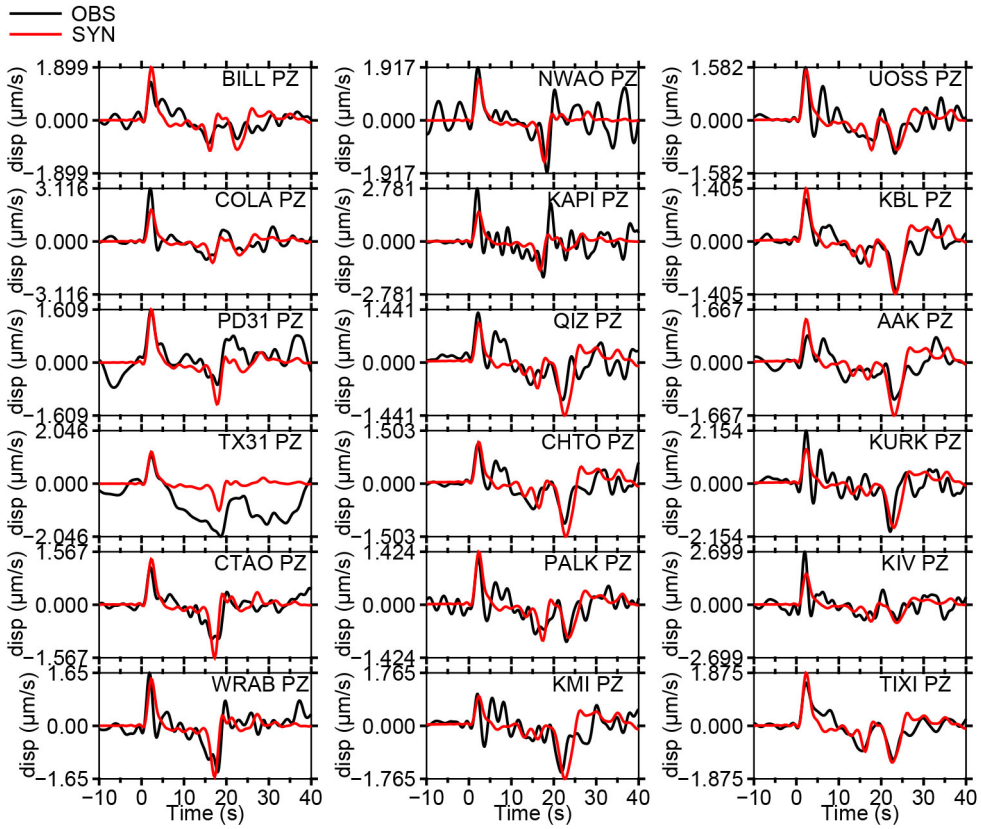

Figure S4

Observed (black) and synthetic teleseismic waveforms (0.01–0.4 Hz) of event F01.

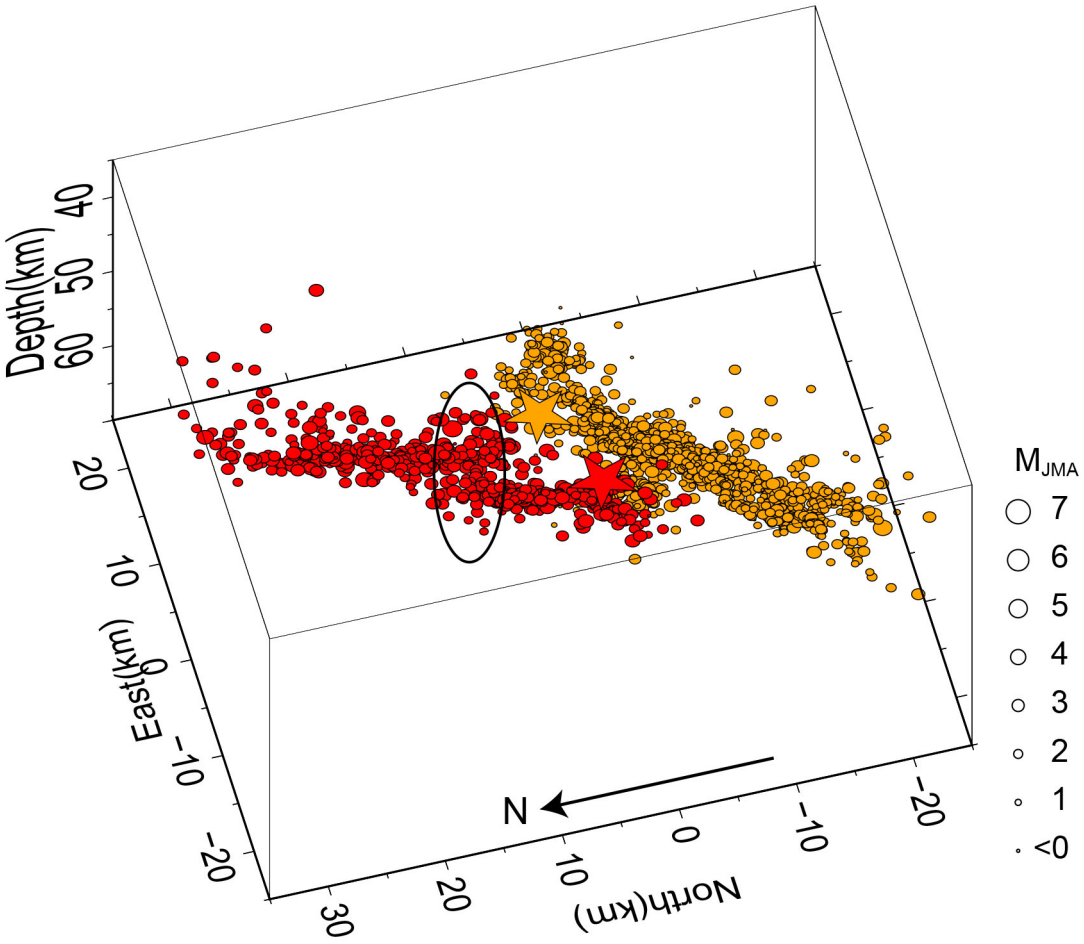

Figure S5

Three-dimensional 24-h aftershock distributions of the 2021 and 2022 earthquakes. The orange star and circles indicate the relocated epicenters of the mainshocks and 24-h aftershocks, respectively, of the 2021 Fukushima-oki earthquake. The red star and circles are for the 2022 earthquake. The black circle shows the location of the possible fault step-over structure.

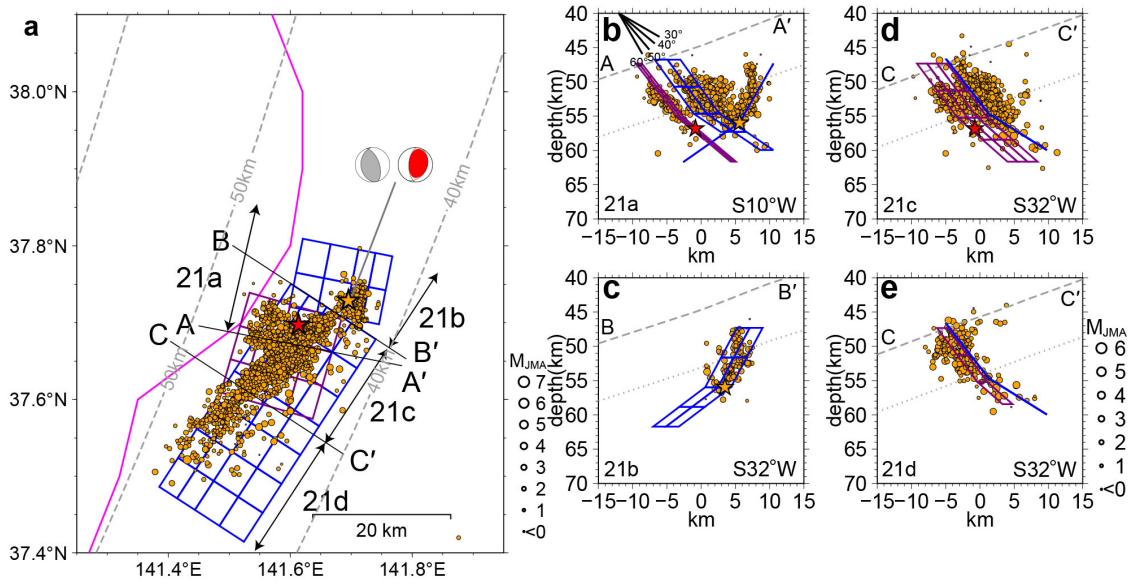

Figure S6

a Another fault model and the relocated 24-h aftershock distribution (orange circles) for the 2021 Fukushima-oki earthquake. **b-e** Their cross sections along lines AA′, BB′, and CC′ for subregions 21a, 21b, 21c, and 21d in Panel **a**. The blue meshes and lines show the preferred fault model. The purple meshes and lines indicate the additional subparallel fault. For each cross-section, the viewing direction is displayed in the lower right corner. Gray-white and red-white focal mechanisms represent the first motion solution by JMA and moment tensor solution from the F-net catalog, respectively. The gray broken lines in Panel **a** denote the plate-boundary depth as in Figure S1. The shapes of the plate boundary along the lines in Panel **a** are shown in the cross-sections. The gray dotted lines represent the surface at a depth of 8.4 km from the plate boundary. The pink line shows the same depth limit as in Figure S1.

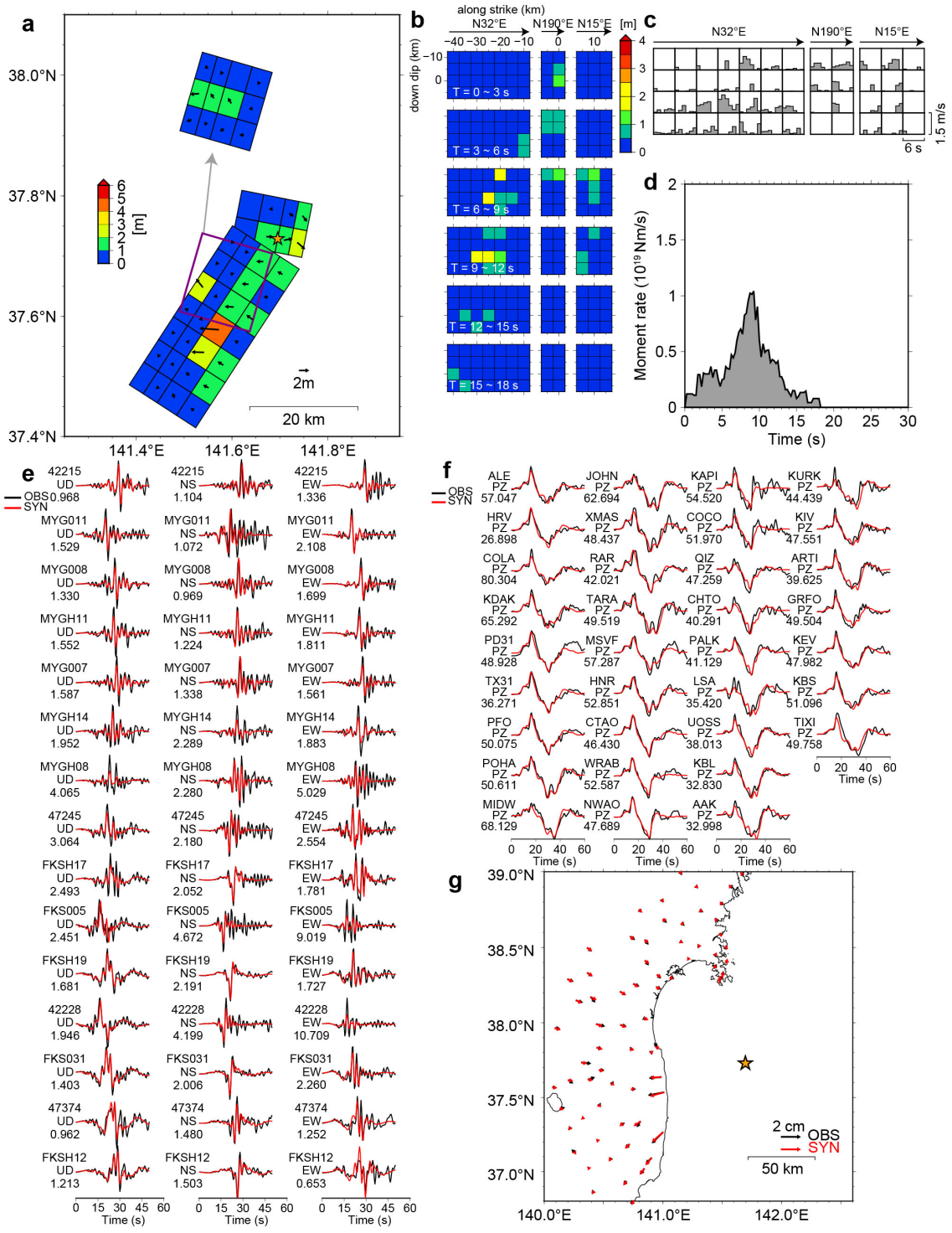

Figure S7

Source inversion results of the 2021 Fukushima-oki earthquake with another fault model.

a Slip distribution. The orange star represents the hypocenter of the 2021 earthquake. The

purple square indicates the location of additional subfaults and the shift of their slip distribution on the map. **b** Snapshots of the slip distribution. **c** Slip rate function of each subfault. **d** Apparent moment rate function. **e, f** Observed (black) and synthetic (red) strong motion velocity waveforms (0.05–0.4 Hz) and teleseismic displacement waveforms (0.01–0.4 Hz). The station name, component, maximum observed amplitude (cm/s for strong motion and μm for teleseismic) are shown to the left of each waveform. **g** Observed (black) and synthetic (red) horizontal static displacements.

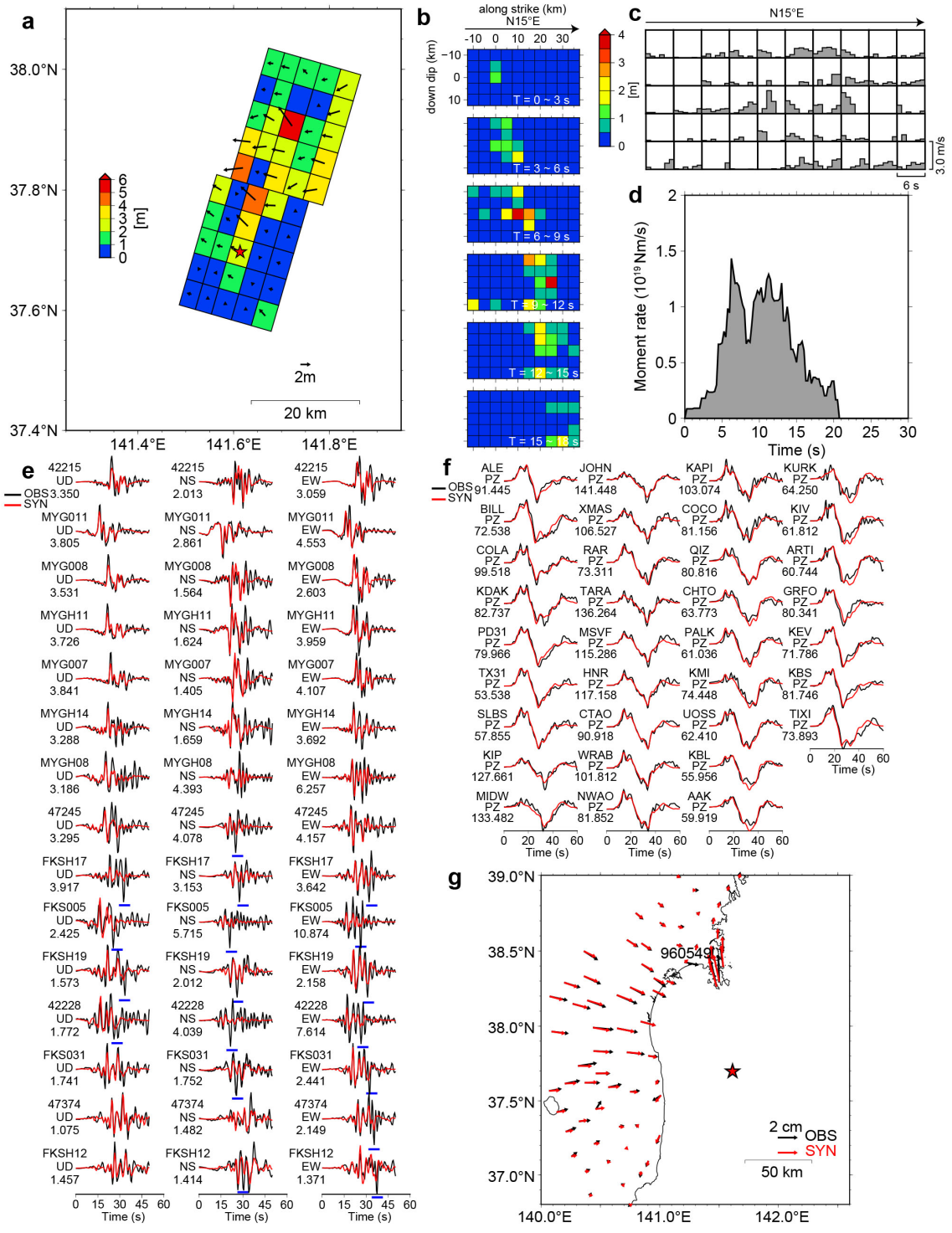

Figure S8

Source inversion results of the 2022 Fukushima-oki earthquake with six time windows. **a** Slip distribution. The red star represents the hypocenter of the earthquake. **b** Snapshots

of the slip distribution. **c** Slip rate function of each subfault. **d** Apparent moment rate function. **e, f** Observed (black) and synthetic (red) strong motion velocity waveforms (0.05–0.4 Hz) and teleseismic displacement waveforms (0.01–0.4 Hz). The thick blue lines indicate the phase where the reproducibility is clearly worse than that in Figure 4. The station name, component, maximum observed amplitude (cm/s for strong motion and μm for teleseismic) are shown to the left of each waveform. **g** Observed (black) and synthetic (red) horizontal static displacements.

Table S1. Datasets used in the inversion analysis.

Dataset	Strong motion	Teleseismic	Geodetic (GNSS)
2021	15 stations 45 components	34 stations 34 UD components	72 stations 72 horizontal components
2022	15 stations 45 components	34 stations 34 UD components	74 stations 74 horizontal components

Table S2. 1D near-source velocity structure model for calculation of the teleseismic Green's functions.

Thickness (km)	Vp (km/s)	Vs (km/s)	ρ (10^3 kg/m^3)
0.20	1.5	0	1.02
0.34	2.0	0.6	2.00
0.17	2.4	1.0	2.15
0.27	2.7	1.3	2.20
0.51	3.2	1.7	2.30
0.49	3.5	2.0	2.35
0.35	4.2	2.4	2.45
8.30	5.8	3.4	2.7
11.80	6.4	3.8	2.8
20.57	7.5	4.5	3.2
∞	8.1	4.6	3.4

Table S3. 1D near-receiver velocity structure model for calculation of the teleseismic Green's functions.

Thickness (km)	Vp (km/s)	Vs (km/s)	ρ (10^3 kg/m^3)
15.0	5.57	3.36	2.65
18.0	6.50	3.74	2.87
∞	8.10	4.68	3.30

Table S4. Source parameters of the medium-sized events.

Event	Origin time (UTC)	Latitude (°)	Longitude (°)	Depth (km)	(Strike,dip,rake) (°)	M_0 (Nm)	Rise time (s)
S01	2021-02-14 07:31:50.29	37.521517	141.431022	49.462	(201, 19, 88)[a]	6.58×10^{16} [a]	1.8[c]
S02	2022-03-18 15:57:48.77	37.735128	141.711344	57.901	(16, 38, 91)[a]	2.02×10^{16} [a]	1.2[c]
F01	2022-03-16 14:34:27.00	37.683923	141.605160	57.493	(22.6, 49, 98.2)[b]	6.31×10^{17} [b]	2.0[d]

a: values are from the F-net moment tensor catalog. b: values are from the Hi-net moment tensor catalog. c: values were obtained by using equation (1) in Ekström et al. (2012). d: value was obtained by trial and error.